Partial Substitution of titanium with tungsten in MIL-167 Metal Organic Framework: Synthesis, Characterization, and Functional Applications

Master's Thesis
Mohammad Azizur Rahman
Intelligent Materials Chemistry
Department of Chemistry
University of Turku
May 2026

The originality of this thesis has been checked in accordance with the University of Turku quality assurance system using the Turnitin Originality Check service. During the preparation of this thesis, artificial intelligence (AI) was used solely for language polishing and grammar checking. All scientific content, data analysis, and conclusions remain the original work of the author.

Master's thesis

Subject: Chemistry

Author(s): Mohammad Azizur Rahman

Title: Partial Substitution of titanium with tungsten in MIL-167 Metal Organic Framework: Synthesis, Characterization, and Functional Applications

Supervisor(s): Ari Lehtonen, Anssi Peuronen

Number of pages: 32 pages

Date: May 2026

Metal–organic frameworks (MOFs) are highly tunable porous materials whose properties can be tailored through the selection of different metal ions and organic linkers. Among them, titanium-based MOFs have attracted significant interest due to their structural stability, high surface area, and potential applications in gas adsorption, separation, and catalysis. In this work, the titanium-based MOF MIL-167 ($Ti(DOBDC)\cdot(Et_2MeNH)_2\cdot nH_2O$), was constructed from Ti^{4+} metal nodes and 2,5-dihydroxyterephthalic acid (DOBDC) linkers. This framework is neutralized by counterions, specifically Et_2MeNH^+, which are essential for charge balance. MIL-167 was modified through partial substitution of Ti with W at varying molar ratios. This modification was motivated by the difference in oxidation states between Ti^{4+} and W^{6+}, which could potentially influence the structural and physicochemical properties of the framework.

Structural characterization using X-ray powder diffraction indicated that the incorporation of W did not significantly alter the crystalline structure of MIL-167. X-ray fluorescence spectroscopy confirmed the presence of tungsten in samples prepared with different Ti precursor substitution levels, although it remains possible that W is located within the pore system rather than being fully incorporated into the framework nodes. Infrared spectroscopy, differential scanning calorimetry, and thermogravimetric analysis showed no substantial differences between the parent and modified MOFs. Nitrogen physisorption measurements revealed negative adsorption behavior, suggesting that the pores of the modified MIL-167 samples were not accessible. The modified MOFs were also evaluated as heterogeneous catalysts for the cycloaddition of CO_2 to epoxides to produce cyclic carbonates; medium catalytic activity was observed. Finally, heterojunctions formed by combining MIL-167 with MIL-125-NH_2 exhibited different UV–Vis reflectance behavior compared to pristine and W-modified MIL-167, suggesting the need for further investigation into their optical properties and potential photocatalytic applications.

Keywords: Metal Organic Framework, organic linker, nitrogen physisorption, heterojunctions, heterogeneous catalyst.

Table of Contents

Abbreviations

MOFs = Metal-organic frameworks

DOBDC = 2,5-dihydroxyterephthalic acid

BET = Brunauer-Emmet-Teller

OMSs = Open metal sites

XRD = X-ray diffraction

XRF = X-ray Fluorescence

IR = Infrared spectroscopy

TGA = Thermogravimetric analysis

1. Introduction

1.1. Metal Organic Framework (MOF)

Porous materials have enabled technologies from simple filters to advanced adsorbents and catalysts [1]. A defining characteristic of these materials is their low density and high void space, which can be engineered with specific functionalities for desired applications. Among porous materials, crystalline structures with long-range order have gained special attention because their structures and properties can be controlled [2].

While synthetic zeolites—composed of inorganic components like silicates and aluminates—have been studying closely since the 1940s, their pore sizes were initially limited. Between the late 1980s and early 1990s, the first crystalline porous materials with pore sizes exceeding 1 and 2 nanometers were reported, respectively [3,4]. A real change occurred in 1995 when Omar Yaghi and colleagues introduced a new class of crystalline porous materials termed metal-organic frameworks (MOFs) [5, 6]. These materials distinguished themselves from earlier coordination polymers through their exceptional stability and permanent porosity, attributed to the strong bonds formed between metal ions and charged organic ligands [7].

MOFs are a type of porous material made from both metals and organic (carbon-based) molecules. They are built from metal clusters connected by organic linkers, as shown in Fig. 1. Both parts are important to the MOF structure. The metal clusters function as connecting nodes, and the organic linkers bridge them into a network [20].

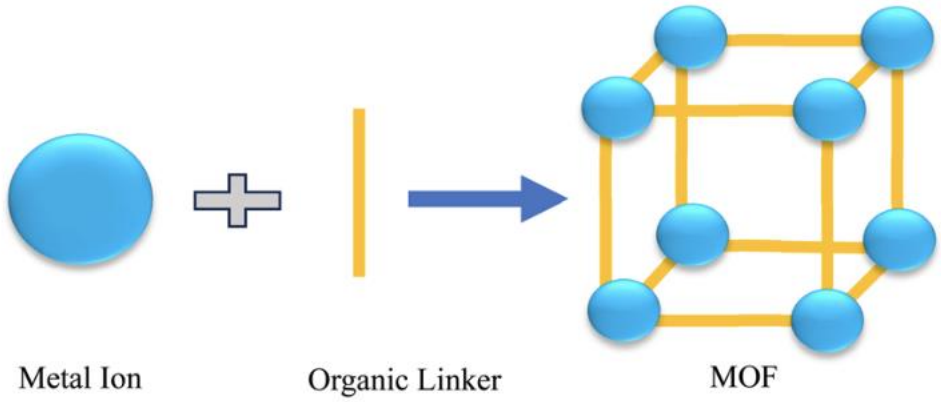

Figure 1. Representation of the basic MOF structure [19].

The pore size in MOFs can be increased in two ways. First, using bigger metal clusters creates larger spaces in the network. Second, using longer organic linkers, which increase the distance between the metal clusters and leads to wider pores and higher porosity [20].

Secondary building units (SBUs) help to classify different MOF structures based on their shape. SBUs are also important for controlling how MOFs are built and for making the frameworks strong and stable [21].

In short, the main features of MOFs are good thermal stability (250–500 °C), large pores, high pore volume, and very high surface area (thousands of m^2 per gram) [22].

The fundamental appeal of MOFs lies in their highly tunable nature, stemming from the nearly infinite combinations of inorganic metal nodes and organic linker molecules. This adaptability has opened a new avenue in the design and application of porous materials. A particularly powerful concept is isoreticular manipulation, which allows for the alteration of a framework's structure and functionality while keeping its underlying topology invariant [8]. This principle is part of a larger design strategy known as reticular chemistry, which has been important for the synthesis and application of porous framework materials like MOFs [9]. The success of this approach is evident in the exponential growth of the field; more than 100,000 structures have been reported in the "MOF subset" of the Cambridge Structural Database (CSD), and the number of MOF-related publications continues to rise every year [10-12].

One of the most notable and enabling characteristics of MOFs is their high porosity. This porosity is conducive to gas storage and separation, catalysis, sensing, biomolecule encapsulation, drug delivery, conductivity, and magnetism. The journey to realizing this porosity has a long history. Although the concept of porosity in extended metal-organic materials was taken into consideration in the late 1980s and early 1990s [1], the first experimental proof via gas adsorption measurements was reported in the late 1990s. Kitagawa and colleagues demonstrated that metal-organic polymers could take up gas-phase guest molecules [13]. An important finding came in 1998 when Yaghi reported the first MOF with proven permanent porosity. Using nitrogen adsorption/desorption isotherms at 77 K and low pressure—a standard procedure for materials like zeolites and porous carbon—his group found out the first values for apparent surface area and pore volume in a MOF [7]. This work marked

a milestone, laying the foundation for achieving and quantifying permanent porosity in these materials [13].

Since those early discoveries, MOFs have become increasingly popular as materials with high surface area. The principles of reticular chemistry have guided the design and development of MOFs. The principles enabled the researchers to create new materials and tailor their pore structures and functionalities with high accuracy [1]. A critical, and often challenging, step is the activation process—the removal of guest molecules (solvents, unreacted linkers) from the pores of as-synthesized MOFs. This step is essential to access the internal pore space, and the development of improved activation methods is equally important as the design of the frameworks themselves [14, 15]. It has often been found that a MOF's Brunauer-Emmett-Teller (BET) surface area can be dramatically increased simply by employing a more sophisticated activation method, such as supercritical CO_2 drying, especially for highly porous or delicate structures [16-18]. As an empirical guideline, while robust MOFs with strong metal-linker bonds (e.g., Zr-carboxylate-based MOFs) can often be activated by conventional thermal methods, more fragile or exceptionally porous frameworks (e.g., Zn-carboxylate MOFs with BET areas >3500 m^2/g) typically require milder techniques like supercritical CO_2 or freeze-drying to avoid structural collapse from capillary forces [2].

it is important to examine the porosity and the methods to properly access it. This thesis aims to build upon this objective. In the following chapters, we will explore the classification and adsorptive measurement of porosity, the critical strategies for activating MOFs to preserve their structural integrity, and the general design principles.

1.2. Metal Organic Framework MIL-167

Structure and Composition

MIL-167 is a well-established titanium-based MOF. It has attracted considerable attention due to its interesting structural properties and potential applications in catalysis, adsorption, and photocatalysis. The framework is built from Ti^{4+} metal nodes connected by organic linkers [23].

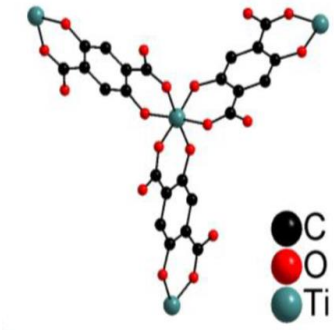

Figure 2. Coordination sphere around the titanium(IV) ions in MIL-167 [23]

Under the solvothermal reaction conditions used to synthesize MIL-167, H_4DOBDC undergoes complete deprotonation. The reaction medium contains N,N-diethylformamide (DEF) and methanol as solvents, with titanium isopropoxide as the Ti^{4+} source. No external base is added [23].

Consequently, the organic linker that binds to the titanium centers is the fully deprotonated form, $DOBDC^{4-}$, not the neutral H_4DOBDC. These groups form strong coordination bonds to the Ti^{4+} centers [23].

The Et_2MeNH^+ cations are not added externally — they are generated in situ during the solvothermal reaction. Specifically, DEF thermally degrades during the synthesis to form diethylamine, which further reacts with methanol to generate diethylmethylamine. These amines are then protonated by H_4DOBDC to form the diethylmethylammonium cations that stabilize the MIL-167 framework. These counterions occupy the pores of the structure [23].

The crystallographic formula of MIL-167 is reported as $Ti(DOBDC)_{1.5}(Et_2MeNH)_2 \cdot nH_2O$. The "1.5" is a stoichiometric average: the crystal structure reveals that for every two titanium(IV) ions, there are three DOBDC linkers, giving an average of 1.5 linkers per titanium atom. The charge balance is achieved as follows: one Ti^{4+} (+4), 1.5 $DOBDC^{4-}$ (-6), and two Et_2MeNH^+ (+2) give a net neutral framework. This is consistent with the crystal structure depicted in figure-2, which reveals that the TiO_6 octahedra are surrounded solely by oxygen atoms from DOBDC ligands, confirming that the linker is fully deprotonated ($DOBDC^{4-}$).

In summary, the shorthand DOBDC indicates the fully deprotonated linker. The presence of diethylmethylammonium counterions (Et_2MeNH^+) further confirms a negatively charged framework, which requires $DOBDC^{4-}$ rather than a partially protonated form [23]. The difference between the linker H_4DOBDC and the actual linker inside the framework $DOBDC^{4-}$ is important to write correct chemical formula of the MOF.

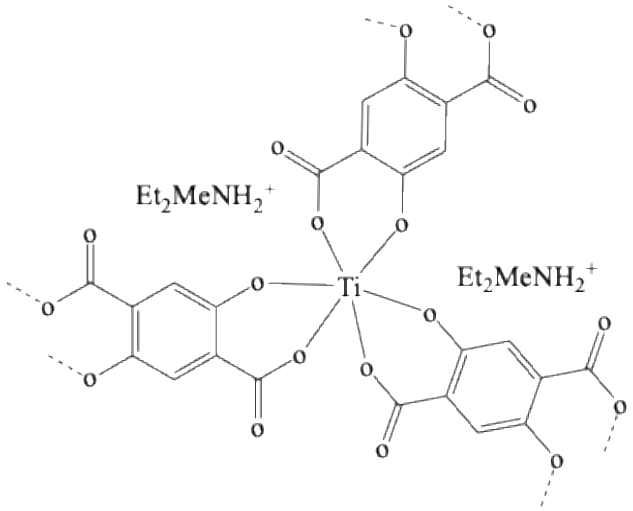

Figure 3. Structure of MIL-167

1.3. Rationale for Metal Substitution in MOFs: Ti(IV) and W(VI)

While pristine MOFs offer excellent performance, there is a continuous drive to enhance their properties for specific applications. One powerful strategy is heterometallic substitution or doping—the partial replacement of a framework metal with a different metal ion. This approach can systematically alter the electronic structure, charge distribution, porosity, and catalytic activity of a MOF without changing its underlying topology [24].

The rationale for substituting titanium with tungsten in MIL-167 stems from the fundamental differences in their chemical properties:

- **Oxidation States:** Titanium is most stable in the +4 oxidation state (Ti^{4+}) [25]. In contrast, tungsten, a Group 6 transition metal, predominantly exists in the +6 oxidation state (W^{6+}) in its stable oxides and complexes [26,27].

- **Ionic Radii:** While both are transition metals, the ionic radius of W^{6+} (approx. 0.60 Å for 4-coordinate) is slightly larger than that of Ti^{4+} (approx. 0.56 Å for 4-coordinate) [28]. This size difference can induce local structural distortions.

- **Charge Distribution:** Substituting a Ti^{4+} center with a W^{6+} center introduces two additional positive charges into the framework [23].

This charge imbalance is the key to the modification strategy. The pristine MIL-167 framework is anionic due to the specific coordination of Ti^{4+} with the deprotonated DOBDC linkers. The framework's negative charge is compensated by the presence of two Et_2MeNH^+ counterions per formula unit [23]. When a Ti^{4+} ion (oxidation state +4) is replaced by a W^{6+} ion (oxidation state +6), the local framework becomes more positive. To maintain overall electroneutrality, the number of charge-balancing Et_2MeNH^+ counterions must decrease.

By reducing the number of bulky counterions occupying the pores, one would expect an increase in the accessible pore volume and potentially an increase in the effective pore size. This could lead to enhanced gas adsorption capacity and altered diffusion properties for guest molecules [24].

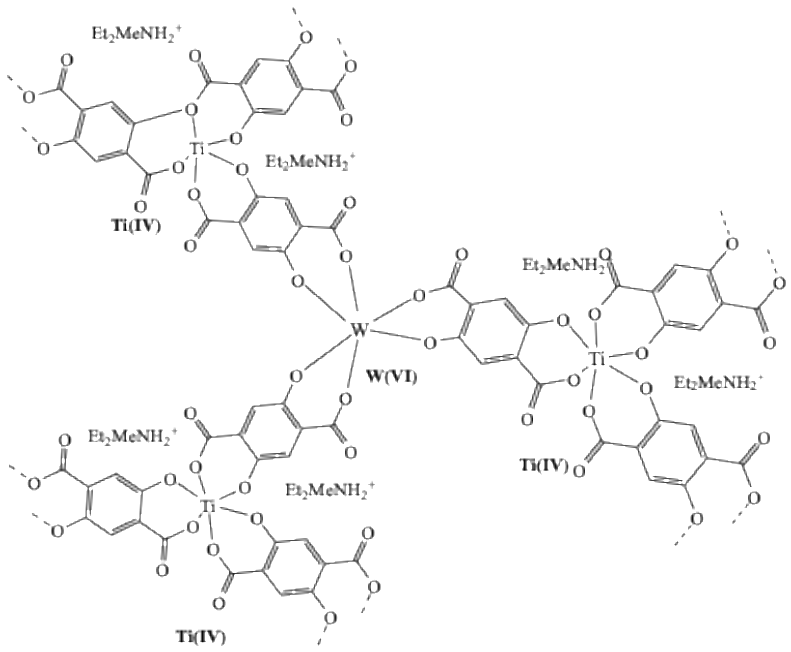

Figure 4. Supposed structure after substitution of a portion of Ti(IV) with W(VI)

1.4. Activation of MOF

The activation of MOFs represents a critical step in accessing their intrinsic porosity, which is fundamental to their performance in applications such as gas storage, catalysis, and separation. As synthesized, MOFs typically contain guest molecules—including solvents, unreacted linkers etc. which may occupy the pore space and must be removed through appropriate activation methods to obtain the material's full surface area and pore volume [1]. The development of effective activation strategies has been a central theme in MOF research, as improper activation can lead to incomplete guest removal or structural collapse.

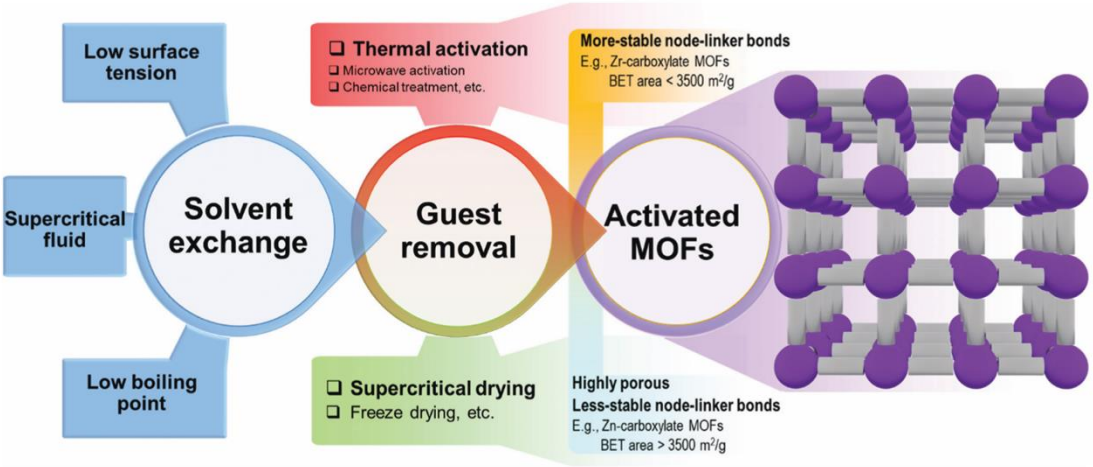

Scheme 1. Overview of the workflow and strategies of MOF activation [1]

As illustrated in Scheme 1 of Zhang et al. [1], the activation workflow typically involves multiple steps, starting from the synthesis of MOFs containing guest molecules, followed by solvent exchange, and finally guest removal via various methods such as thermal activation, supercritical CO_2 drying, freeze drying, microwave activation, or chemical activation. The choice of activation method depends critically on the stability of the MOF and its porosity regime.

Zhang et al. [1] provide a comprehensive historical overview of MOF activation methodologies, highlighting that thermal activation under vacuum following solvent exchange is the commonly employed approach. The authors emphasize that exchanging high-boiling-

point solvents (e.g., DMF) with low-surface-tension solvents such as acetone or methanol before thermal treatment is commonly used for most MOFs. As a general empirical guideline summarized in Scheme 1, thermal activation is viable for MOFs with more stable node-linker bonds (e.g., Zr-carboxylate-based MOFs) or BET areas smaller than 3500 $m^2 \cdot g^{-1}$, while supercritical drying is recommended for less stable or highly porous MOFs [1].

In the present work, a thermal activation protocol was followed. Specifically, the procedure involved washing synthesized MOF samples with chloroform, followed by solvent exchange and thermal treatment at 130 °C for 24 hours. A parallel activation was conducted using acetone as the exchange solvent.

1.5. Physisorption of gases

Characterizing porous solids and fine powders relies heavily on gas adsorption measurements. Nitrogen physisorption at 77 K – the boiling point of liquid nitrogen – is the standard method for obtaining specific surface area, pore volume, and pore size distribution. The underlying principle is physical adsorption: nitrogen molecules adhere to a solid surface via van der Waals forces. This process is reversible and occurs whenever a gas contacts an adsorbent surface [29].

The 2015 IUPAC report reviewed the 1985 guidelines and stated that physisorption arises from the same intermolecular forces that cause vapor condensation. Beyond the usual dispersion and repulsive forces, more specific interactions (polarization, field-dipole, field gradient-quadrupole) can arise depending on the adsorbent's surface chemistry and the adsorptive's electronic structure. Nitrogen has a significant quadrupole moment, so its adsorption depends not only on pore geometry but also on surface functional groups [29].

To obtain a physisorption isotherm, the adsorbed gas amount is measured as a function of equilibrium pressure at constant temperature. For nitrogen at 77 K (below its critical temperature), the relative pressure p/p^0 is used, where p^0 is the saturation vapor pressure. The resulting isotherms fall into several IUPAC-classified types, each giving qualitative information about the material's porous structure [29].

Specific surface area is derived by using the Brunauer-Emmett-Teller (BET) method. Despite known theoretical limitations, BET remains the standard. The linear form of the BET equation is:

$$\frac{p/p^0}{n(1-p/p^0)} = \frac{1}{n_m C} + \frac{C-1}{n_m C}(p/p^0) \qquad \text{(Eq. 1)}$$

Here, n is the amount adsorbed at relative pressure p/p^0, n_m is the monolayer capacity, and C is a constant related to the adsorption energy. From n_m, the specific surface area a_s(BET) follows:

$$a_s(\text{BET}) = n_m \cdot L \cdot \sigma_m \qquad \text{(Eq. 2.)}$$

where L is Avogadro's number and σ_m is the molecular cross-sectional area of the adsorbate. For nitrogen, σ_m = 0.162 nm² is conventionally used (close-packed monolayer assumption) [29].

MOFs are hybrid materials as inorganic clusters are connected by organic linkers [23]. So, they have extremely high surface areas and tunable pores, but they also challenge conventional physisorption analysis [29].

The quadrupole moment of nitrogen is a primary source of difficulty. It causes specific interactions with exposed ions and surface groups and can change both the orientation of adsorbed molecules and the micropore filling pressure. For many zeolites and MOFs, adsorption begins at extremely low relative pressures (down to ~10^{-7}), where diffusion is slow and equilibrium is hard to reach [29].

1.6. MOF/MOF Heterojunctions

Sunlight-driven photocatalysis offers a renewable route to fuels, bypassing fossil sources. However, only a small fraction of solar photons falls into the ultraviolet (UV) region; most are in the visible (Vis) and infrared (IR) ranges. To use abundant solar energy efficiently, a photocatalyst needs a narrow band gap (below about 2.95 eV) to absorb a large portion of the spectrum. Beyond light harvesting, there are two other factors like separating photogenerated charge carriers and moving them to reactive sites before they recombine. This is why many

photocatalytic systems rely on metal nanoparticles or molecular complexes to suppress electron–hole recombination [30].

An alternative approach, as like photocatalysis, is to combine two materials into a heterojunction. If their band structures are carefully matched, the resulting interface can enhance visible-light absorption and charge separation at the same time. MOFs are attractive for this purpose. Their structural tunability allows researchers to adjust optoelectronic and catalytic properties, and their intrinsic porosity facilitates diffusion of reactants and products [30].

However, there are some challenges in MOF photocatalysis as in conventional systems to achieve both a narrow band gap and efficient charge separation. By following the semiconductor heterojunctions, several scientists have started combining different MOFs with each other. Though most studies have focused on MOF–semiconductor or MOF–covalent organic framework (COF) hybrids, rather than MOF–MOF pairs [30].

For a MOF/MOF composite to qualify as a true heterojunction, electronic interactions between the two components must alter the optical and electronic properties of the mixture. In an ideal case, a well-constructed MOF/MOF heterojunction would simultaneously offer extended visible-light harvesting, high charge separation efficiency, enhanced catalytic activity, and retained porosity. Understanding how these optoelectronic properties affect photocatalytic performance is crucial for designing better MOF-based photocatalysts. A successful system of this type could eliminate the need for expensive co-catalysts or dye photosensitizers [30].

Among Ti-based MOFs, MIL-125-NH_2 is one of the best-performing photocatalysts. It absorbs light into the early visible region (< 500 nm) and shows high activity for water reduction. MIL-167 is another stable Ti-MOF, but it absorbs light up to approximately 700 nm – further into the visible range. Because their absorption profiles are complementary, combining MIL-167 with MIL-125-NH_2 is a good strategy. The resulting heterojunction reportedly shows improved optoelectronic properties and efficient charge separation [30].

The laboratory dedicated for this experiment under the thesis does not have instrument for measuring UV-Vis absorbance directly. Instead, a Cary 60 spectrometer equipped with a diffuse

reflectance accessory was used. This setup measures the light reflected from the surface of powder samples.

To examine the absorbance, the reflectance data was converted by using the Kubelka–Munk function, which converts reflectance into a quantity proportional to the absorption coefficient [31].

The Kubelka–Munk function is defined as:

$$F(R_\infty) = \frac{(1-R_\infty)^2}{2R_\infty} \qquad \text{(Eq. 3)}$$

Here, $R\infty$ is the diffuse reflectance of an opaque (infinitely thick) sample, expressed as a fraction between 0 and 1. The resulting $F(R\infty)$ value, typically plotted in arbitrary units, behaves like an absorbance spectrum [31].

Therefore, the measurements were done for the reflectance of each MOF against a $BaSO_4$ white reference. The raw reflectance spectra were then converted to $F(R\infty)$ using the equation above. This approach allowed to compare the optical properties of pristine MIL-167, W-doped MIL-167, and the MIL-167/MIL-125-NH_2 heterojunctions despite having no direct absorbance measurement capability.

1.7. Chemical Conversion of CO_2 to Cyclic Carbonates by MOFs

CO_2 from fossil fuel combustion is a major greenhouse gas, and its rising atmospheric concentration has driven decades of environmental concern. Reducing emissions requires effective capture and sequestration (CCS) technologies. Researchers have tested many materials for CO_2 capture, like zeolites, porous organic polymers, amine-based solvents, and more recently metal-organic frameworks (MOFs). An attractive extension of capture is to convert the absorbed CO_2 directly into useful chemicals. This approach turns a waste stream into a feedstock, which is valuable both industrially and academically [32].

CO_2 is thermodynamically stable and kinetically inert, so fixing it into other molecules is very difficult. Moreover, CO_2 is cheap, non-toxic, and abundant. Porous MOFs are promising here because their structures and pore chemistries can be utilized. With appropriate design, MOFs can convert CO_2 into dimethyl carbonate, cyclic carbonates, or formic acid.
Cyclic carbonates are industrially important. Traditionally, they are made using highly toxic phosgene. A greener alternative is the catalytic coupling of CO_2 with epoxides, which inserts CO_2 into the C–O bond of the epoxide ring without generating by-products [32].

Several strategies improve CO_2 capture in MOFs, including creating open metal sites (OMSs) and attaching functional groups to the linkers. MOFs are particularly well suited for combined capture and conversion because they can act as both adsorbents and heterogeneous catalysts. The OMSs bind CO_2 and function as Lewis acid sites to activate epoxides. Meanwhile, the pores hold the epoxide molecules close to the reactive sites [32].

Some MOFs catalyze cyclic carbonate formation efficiently, but usually under harsh conditions: temperatures above 80 °C and pressures above 2 MPa. Such conditions demand high energy input. Only a few MOFs — for example MMFC-2, MMPF-9, and HKUST-1 — work well under mild conditions. Developing new MOFs that perform this reaction at lower temperatures and pressures remains an important goal [32].

Four features of MOFs are important: good chemical and thermal stability, high CO_2 adsorption capacity and selectivity, a high density of Lewis or Brønsted acidic sites (OMSs being the most common), and — ideally — tubular channels to facilitate mass transport of reactants. Designing and synthesizing MOFs that combine all these features is an active area of research [32].

2. Experimental section

All chemicals were obtained commercially and used without any further purification. A solution of tungsten triethylene glycolate, $W(eg)_3$ (where eg = ethylene glycolate dianion, $–OCH_2CH_2O–$), in ethylene glycol was prepared following a published procedure [33]. In this case, no distillation was done. The concentration of the solution is 0.4 M.

2.1. Synthesis

MIL-167 was synthesized using 20 mL Teflon autoclave liner following the published procedure [23] with different amounts of substances and volumes. Later, different mol-% of Ti precursor was replaced by W.

MIL-167: $Ti(DOBDC)_{1,5}(Et_2MeNH)_2 \cdot nH_2O$

Initially MIL-167 was synthesized using 25 mL Teflon autoclave liner [23]. Later, 20 mL Teflon lined Parr autoclave was used as follows:

1.27 g (6.40 mmol) of 2,5-dihydroxyterephtalic acid, 1.76 mL of N,N-diethylformamide and 1.76 mL of methanol were introduced in a 20 mL Teflon autoclave liner. The mixture was stirred with a magnetic bar at room temperature. The magnetic bar was removed and 0.47 mL (1.58 mmol) of titanium isopropoxide was added slowly in the mixture, leading to a dark red precipitation. The reactor was then sealed, placed in an oven, and heated at 180 °C for 24 h (heating rate: 150°C h^{-1}) and further it was let cool down to room temperature. The resulting deep red solid was recovered by filtration, repeatedly washed with diethyl ether followed by N,N-dimethylformamide and dried at room temperature.

Modification of MIL-167

The above synthesis of MIL-167 was repeated by replacing 5, 10, 15, 30, 40, 50,70, 90 mol-% of Ti precursor by W from solution of $W(eg)_3$ in ethylene glycol.

The volumes of $Ti(OiPr)_4$ and the solution of $W(eg)_3$ in ethylene glycol were taken as given in Table 1.

Table 1. Volumes of $Ti(OiPr)_4$ and the solution of $W(eg)_3$ in ethylene glycol for replacement of Ti with W.

Replacement %	**$Ti(OiPr)_4$**	**Solution of $W(eg)_3$ in ethylene glycol**
5	0.45 mL (1.51 mmol)	0.20 mL (0.08 mmol)
10	0.43 mL (1.43 mmol)	0.40 mL (0.16 mmol)
15	0.40 mL (1.35 mmol)	0.60 mL (0.24 mmol)
30	0.33 mL (1.11 mmol)	1.20 mL (0.48 mmol)
40	0.29 mL (0.96 mmol)	1.60 mL (0.64 mmol)
50	0.24 mL (0.80 mmol)	2.00 mL (0.80 mmol)
70	0.15 mL (0.48 mmol)	2.80 mL (1.11 mmol)
90	0.05 mL (0.16 mmol)	3.60 mL (1.43 mmol)

Moreover, modification of MIL-167 was done by keeping the amount of titanium isopropoxide fixed and adding 0.050 mL (0.020 mmol), 0.075 mL (0.030 mmol), 0.100 mL (0.040 mmol), 0.125 mL (0.050 mmol) of tungstic acid and ethylene glycol solution.

Modification of MIL-167 was also done with ethylene glycol in absence of co-solvent methanol. The experiment was done for 15- and 30-mol% replacement. For 15- and 30-mol% replacement 1.16 mL and 0.56 mL of ethylene glycol was added respectively instead of methanol as co-solvent.

2.2. Activation

To activate the samples, initially 300 mg of sample and 10 ml of chloroform were used. Firstly, the samples were filtered out with chloroform and then new chloroform was added. Then the samples were left to soak in chloroform in round bottom flask for the weekend. Thereafter, the

chloroform was filtered out, and the samples were heated at 130 ºC under a reduced pressure for 24h. A similar activation was done with acetone. In this case, 300 mg of samples were filtered out with acetone. Then the samples were left to soak in 10 mL of acetone overnight. Then the acetone was filtered out, and the sample were heated at 130 ºC under a reduced pressure for 24h.

2.3. MIL-167/MIL-125-NH_2 heterojunctions

MIL-125-NH_2 was synthesized based on reported procedures [30] as follows:

The linker 2-aminobenzene-1,4-dicarboxylic acid (0.1 g) was dissolved in 4.0 mL of N,N-dimethylformamide and 1.0 mL of methanol. After stirring, 0.1 mL of titanium isopropoxide was added to the mixture and it was sonicated for 5 min. Then, the suspension was heated up to 120 °C for 72 h. The obtained yellow powder was first washed several times with N,N-dimethylformamide, then stirred overnight in methanol, and washed several times with methanol. Finally, the obtained powder was dried at 60 °C for 5 h.

5% and 10%- W doped MIL-167/MIL-125-NH_2 heterojunctions were made as above except 10 mg of each sample was introduced in MIL-125-NH_2 precursor solution, prior to heating.

2.4. Characterization

The X-ray diffraction patterns of the samples were measured using a PANalytical Aeris diffractometer equipped with a copper (Cu) X-ray tube and PIXcel1D-Medipix3 detector. The measurements were performed with Cu Kα radiation at 40 kV and 7.5 mA. The instrument setting included a 1/8° divergence slit. The measurement was done in advanced mode and the measurement program was selected as MOF_4x11 mins and zero background sample holder was used. The phase identification was done using PANalytical HighScore Plus software, which compared the experimental diffraction patterns with reference patterns from the ICDD PDF-4+ database to determine phase compositions of the samples.

X-ray fluorescence spectroscopy was used to determine the elemental composition of the sample and its corresponding concentrations (% and ppm). The instrument - PANalytical

Epsilon 1 featured an internal Omnian calibration, a 50 kV silver-anode X-ray tube with Kα emission around 22 keV, and an SDD5 detector. The powdered sample was placed inside a holder having a clear film sealed across its bottom, and then the holder was put inside the instrument's sample chamber. Thereafter the measurement was done with academia 10 min setting under advanced mode.

IR spectra were collected with Bruker Vertex 70 equipment and OPUS software. The UV-Vis reflectance spectra were collected with Cary 60 UV-Vis Diffuse Reflectance Accessory. $BaSO_4$ was used as white reference.

TGA-DSC measurement was done using TA Instrument SDT-Q600. Air was used as purge gas in the analysis. Ramp 10ºC/min to 800ºC was used as the heating parameter.

For nitrogen physisorption, the methodology was divided into three steps to assess the materials properly. The first step was an ex-situ pre-treatment, followed by an in-situ pre-treatment, and lastly the adsorption and desorption analysis to determine the characteristics of the samples. Before physisorption analysis, all samples were degassed under vacuum to remove any adsorbed moisture or contaminants.

For the experiment with MIL167_15%-W and UIO-66, 50 mg of each sample was taken. Later, the analysis was done on MIL-167, MIL-167_5%-W, MIL-167_10%-W, MIL-167_30%-W, and this time 100 mg of each sample was taken. The sample was placed in pre-weighed sample tubes and heated to 180 °C under vacuum for approximately 12 hours. This degassing process ensured that all adsorption sites were clean and accessible to nitrogen molecules during the measurement. After the degassing step, the samples were reweighted to determine the dried weight used in the analysis.

Nitrogen adsorption-desorption isotherms were measured at 77 K using surface area and porosity analyzer (micromeritics). After the degassing process, the sample tubes were transferred to the analysis port of the instrument, where a pretreatment step was carried out. A heating mantle was placed over the tubes, and the samples were heated in situ for approximately 2 hours to remove any residual moisture or atmospheric contaminants that may have been re-absorbed during handling. Following this pretreatment, the samples were allowed to cool to

room temperature, and the analysis ports were then immersed in liquid nitrogen to conduct the nitrogen physisorption measurements at 77 K.

2.5 Chemical Conversion of CO_2

The experiment for catalytic conversion of CO_2 to cyclic carbonate was done following the published procedure [32] as follows: 10.00 mg of MIL-167, 2.27 mL of styrene oxide, 10 mg of tetra butylammonium bromide were mixed in a two neck round bottom flask. CO_2 was added from a balloon attached to one neck. The reaction was done with stirring for 48h at 60 °C. For the ^1H NRM analysis, in the NMR tube 600 µL deuterated chloroform was taken and a very small amount of samples were collected from the flask with a syringe.

3. Results and Discussion

Initially MIL-167 was synthesized using 25 mL and 20 mL Teflon autoclave liner. Difference between the XRD patterns of MIL-167 prepared using 25 mL and 20 mL Teflon autoclave liner is given in the Figure 5:

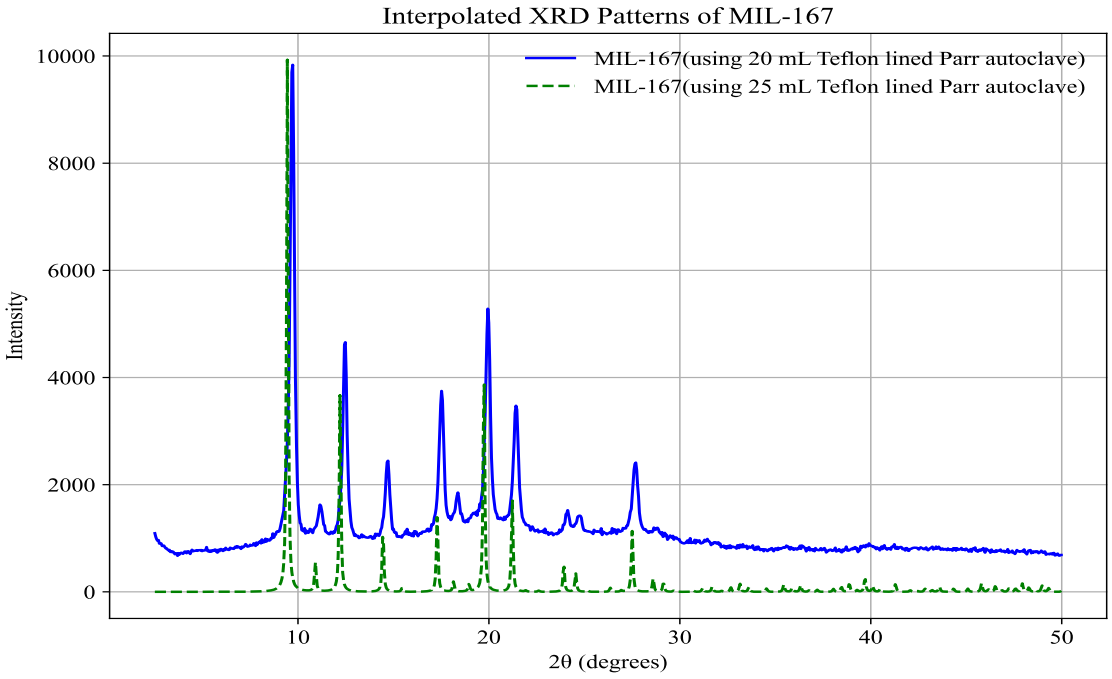

Figure 5. Comparison of XRD patterns of MIL-167 using 25 mL and 20 mLTeflon autoclave liner

From Figure 5, X-ray powder diffraction patterns of MIL-167 synthesized using either 25 mL or 20 mL Teflon autoclave liner were found almost identical. When MIL-167 was prepared with 20 mL Teflon lined Parr autoclave, the intensity peak shifted slightly towards right (higher 2θ angle). It can be said that change in size of autoclave does not change the crystal structure of original MOF significantly. But a smaller autoclave volume could lead to higher internal pressure during solvothermal synthesis. This can affect crystal growth, cause slight structural contraction and lead to peak shifts toward higher angles.

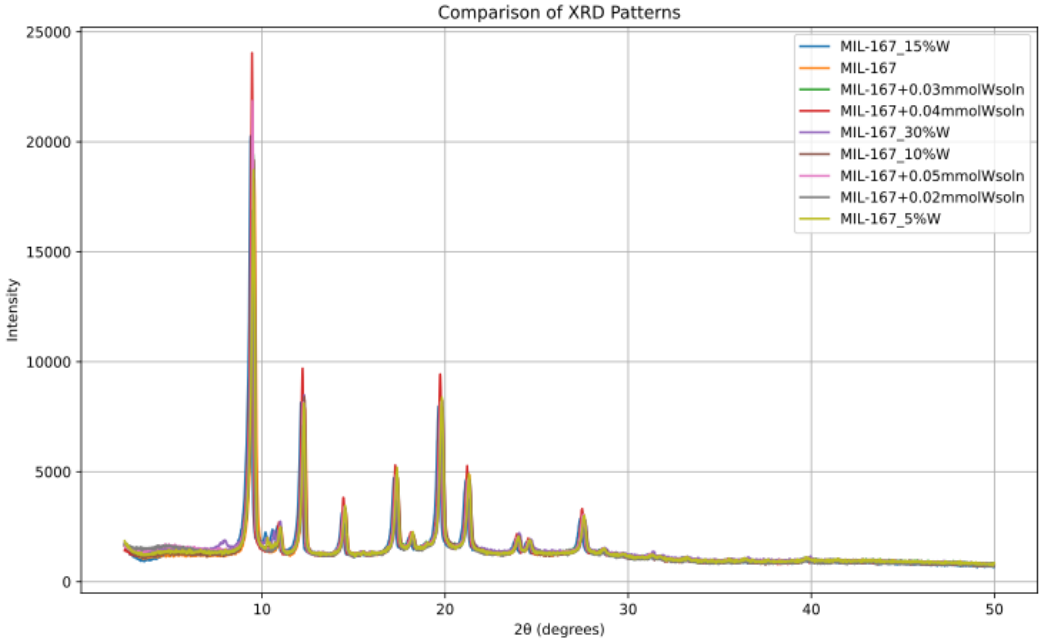

Figure 6. XRD patterns of MIL-167 and supposed W-doped-MIL-167 sample

From Figure 6, the XRD patterns of MIL-167 and supposed W-doped-MIL-167 reveal that the doping of W does not alter the crystal structures of W-doped modified MIL-167.
However, the crystals of MOFs can be obtained up to 30% mol substitution of W; no crystal was found beyond that mol-% of substitution. Further investigation is required to find out the reasons why beyond 30% mol substitution of W does not yield any crystal.

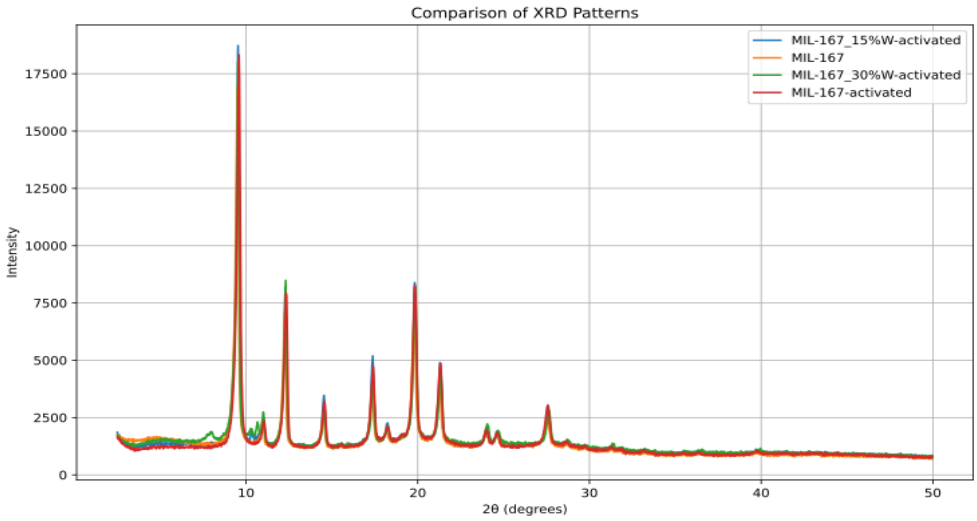

Figure 7. XRD patterns of MIL-167 and supposed W-doped-MIL-167 samples activated with chloroform

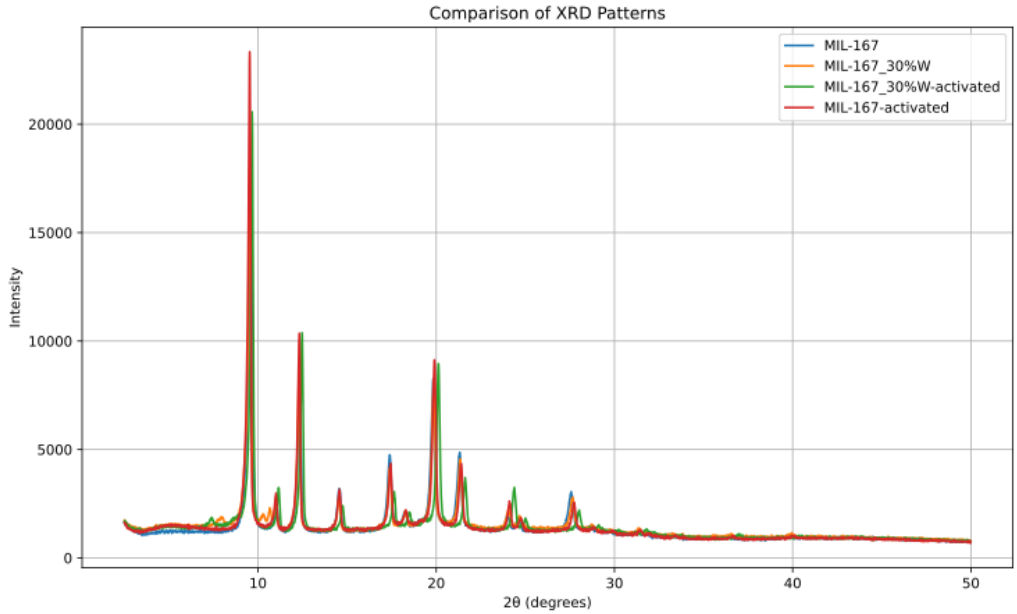

Figure 8. XRD patterns of MIL-167 and supposed W-doped-MIL-167 samples activated with acetone

To ensure that the activation procedure (chloroform or acetone soaking followed by heating under vacuum) does not alter the crystal structure of MIL-167 and W-doped-MIL-167 samples, XRD patterns before and after activation were compared. As shown in Figures 7 and 8, identical patterns were observed, confirming that the activation conditions do not affect the

structure of the framework. This is consistent with the rigid nature of MIL-167 reported in the literature [23].

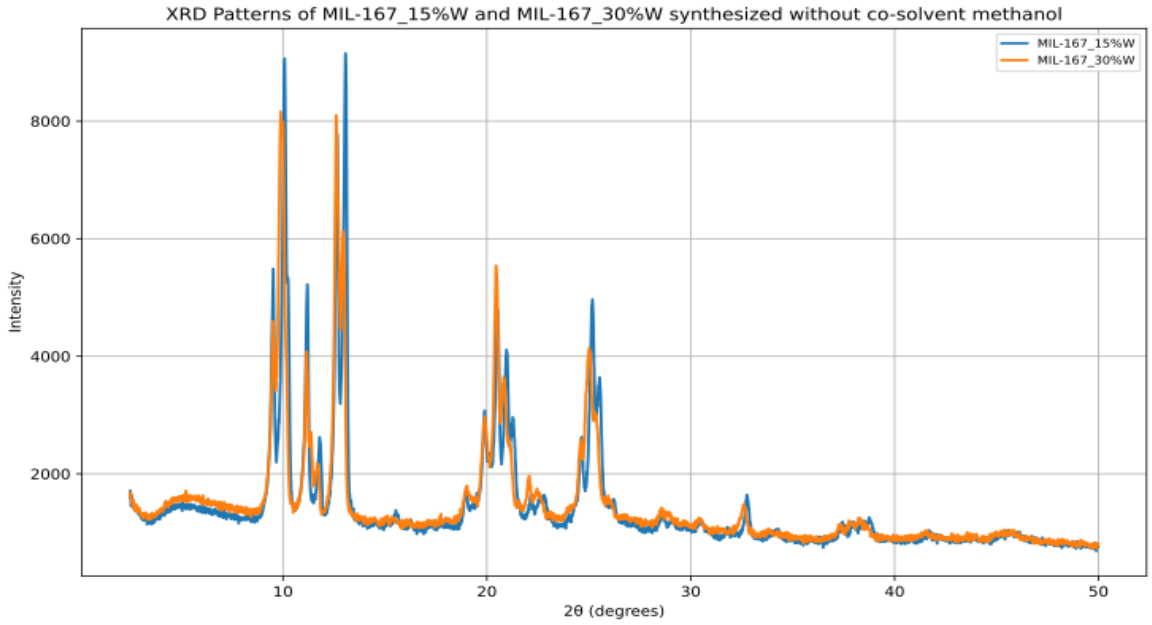

Figure 9. XRD patterns of MIL-167_15%-W and MIL-167_30%-W synthesized without co-solvent methanol.

The XRD patterns of MIL-167_15%-W and MIL-167_30%-W synthesized without co-solvent methanol is shown in Figure 9. The experiment was conducted to investigate whether it is possible to synthesize the MOF without co-solvent methanol. A brick reddish crystal powder was found in absence of methanol. So, it is assumed that methanol has a specific role in the formation of crystal. Further research is required to identify the role of methanol in detail and the composition of the mixtures.

Table 2. Composition of Ti and W in supposed modified MIL-167

Element	**Composition Ti and W**				**Unit**
	5%	**10%**	**15%**	**30%**	
Ti	88.38	86.68	84.63	79.91	%
W	8.91	10.81	12.74	18.39	%

From Table 2, X-ray fluorescence spectroscopy confirms the presence of W in all samples with varying mol-% replacement of the Ti precursor. This indicates the presence of tungsten into the material. However, XRF does not distinguish whether W is incorporated into the lattice or present as extra-framework species. If not lattice-substituted, tungsten is more likely present as

dispersed tungsten oxide (WO_x) species or may be as polyoxotungstates, rather than as isolated W^{6+} ions.

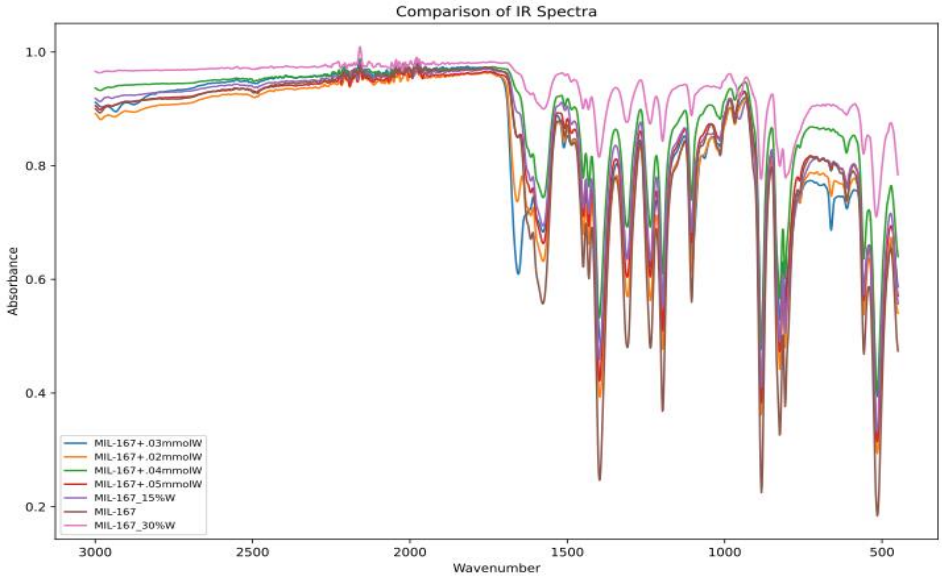

Figure 10. IR spectra of MIL-167 and supposed W-doped-MIL-167 samples

As shown in Figure 11, with infrared spectroscopy, no significant dissimilarities except around 1600 cm^{-1} are found in the IR spectrum of MIL-167 and supposed W-doped-MIL-167 samples. The absence of trough at around 1600 cm^{-1} for the supposed modified MIL-167 could not be interpreted and further investigation is required.

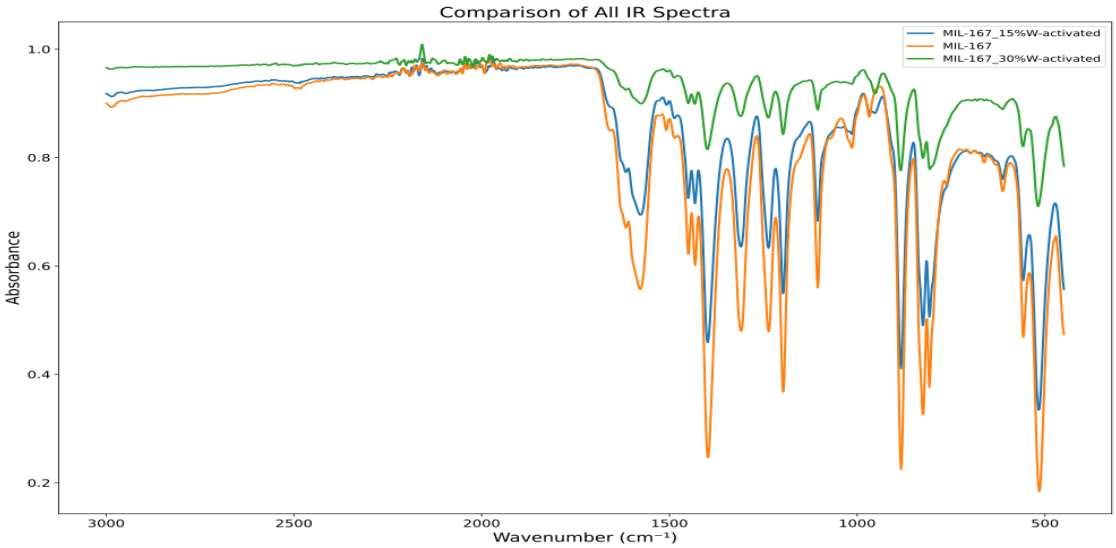

Figure 11. IR spectra of MIL-167 and supposed W-doped-MIL-167 samples activated with chloroform

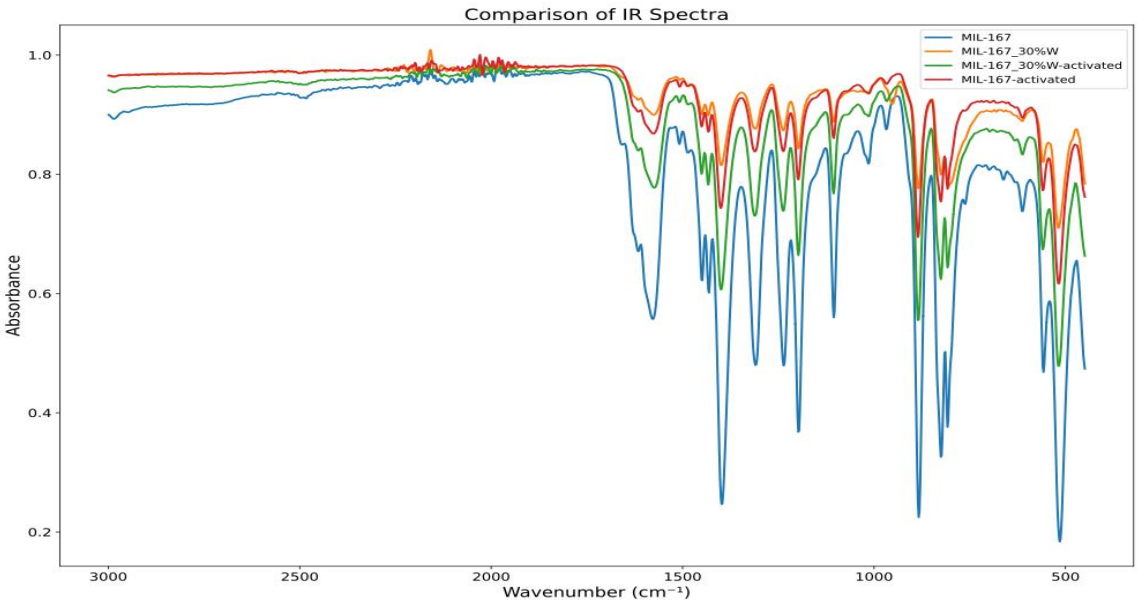

Figure 12. IR spectra of MIL-167 and supposed W-doped-MIL-167 samples activated with acetone

In Figure 11 and 12, the carbonyl C=O stretch of N,N-diethylformamide is found around 1600 cm^{-1} , therefore, upon activation the C=O band is supposed to decrease or disappear, but it did not happen. So, the samples might not have been activated.

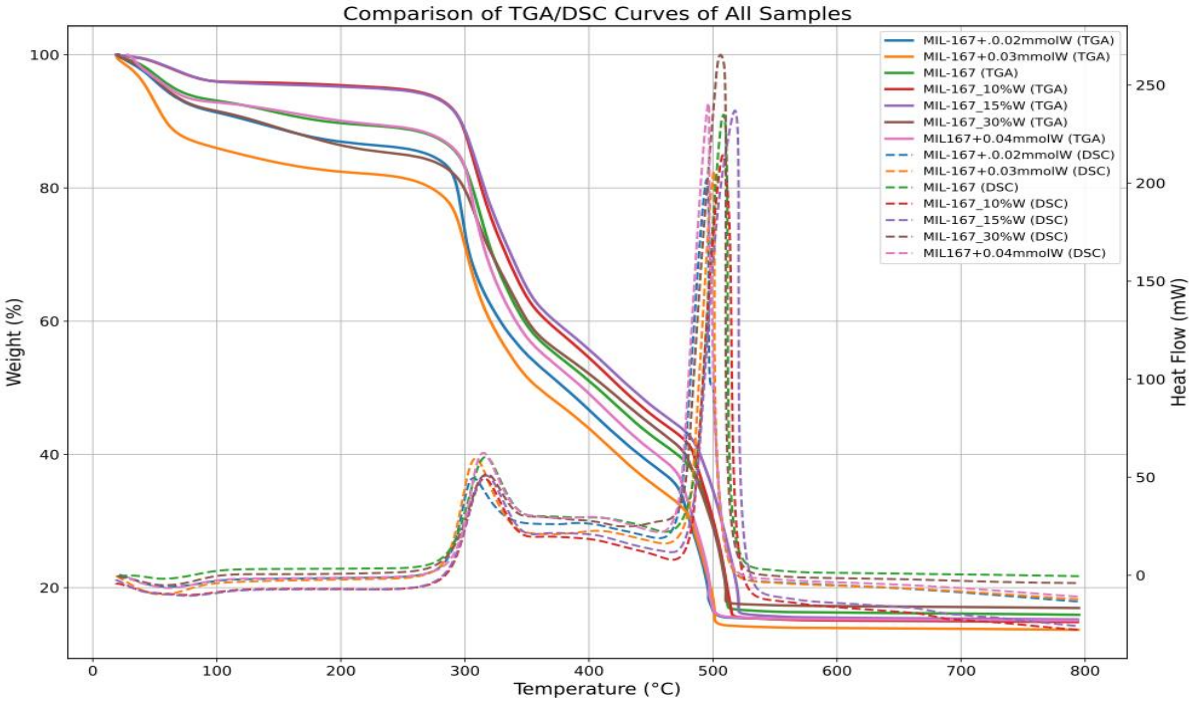

Figure 13. TGA/DSC curves of MIL-167 and supposed W-doped-MIL-167 samples

From Figure 13, the TGA curves of all samples show an initial weight loss below 100 °C, caused by the removal of physically adsorbed water. A second weight loss between 100 and 300 °C may correspond to the release of guest DEF molecules from the pores, with variations indicating differences in solvent content among the samples. A major weight loss above 300 °C may be associated with the decomposition of the organic linker and collapse of the MIL-167 framework, accompanied by an exothermic peak in the DSC curves. The residual mass at higher temperatures is attributed to the formation of metal oxides (TiO_2 and WO_x).

The TGA/DSC curves of the samples revealed no significant changes of the physical and chemical phenomena which are associated with mass changes and /or heat changes.

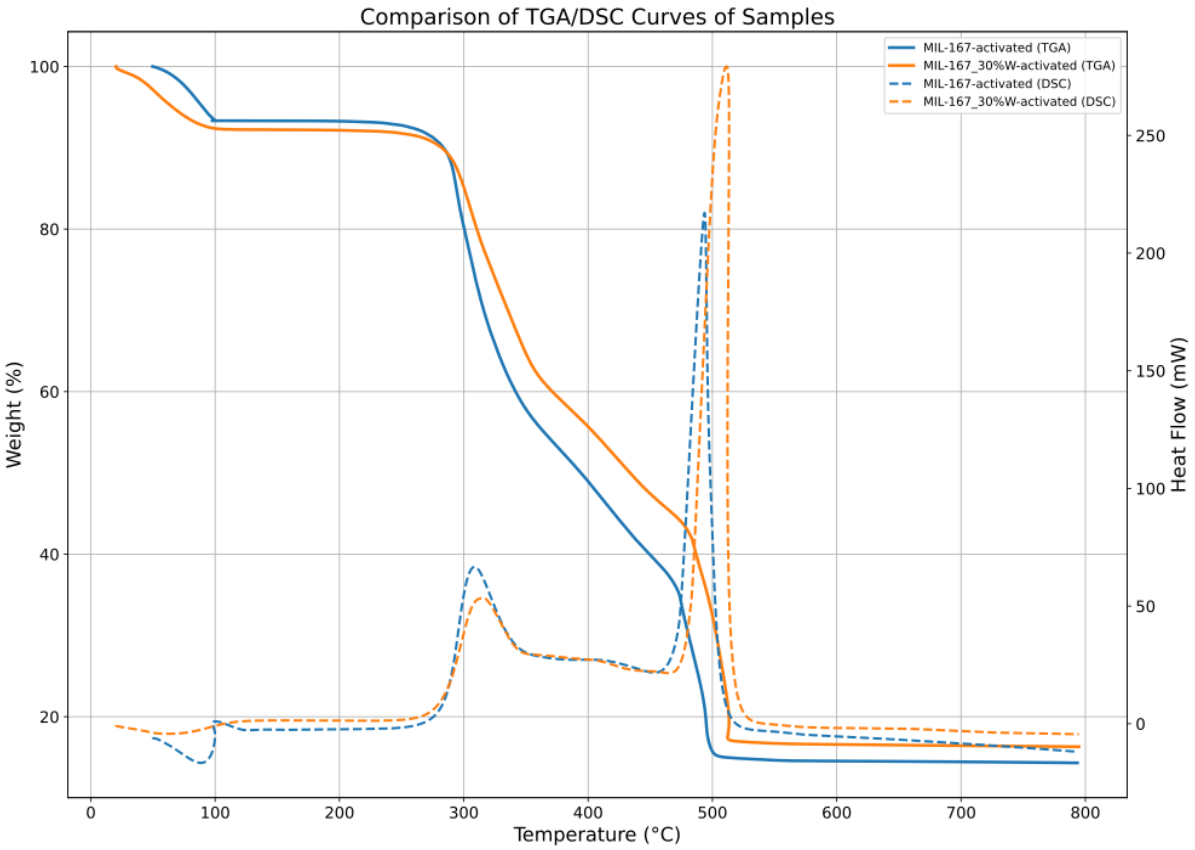

Figure 14. Interpolated TGA/DSC curves of sample activated with acetone solution

As shown in Figure 14, the TGA/DSC curves of the activated samples are nearly identical to those of the non-activated samples shown in Figure 14, indicating that the activation procedure does not alter the thermal decomposition behavior of the MIL-167 framework.

The samples were activated with both chloroform and acetone solvents. With chloroform, no significant changes were found with XRD, IR characterization techniques among activated and non-activated samples. Later the samples were activated with acetone exchange solvent, though no significant changes were found with XRD, IR and TGA/DSC characterization technique among the activated and non-activated samples. But in the nitrogen physiosorption technique, without activation, during the degassing process of nitrogen physiosorption, white crystalline powder was found inside the tube. But after activating the sample with acetone exchange solvent, very little amount of crystalline powder was found inside the tube. It is assumed that after the activation process there were some volatile compounds present in the sample; however, acetone could act as solvent for the activation process.

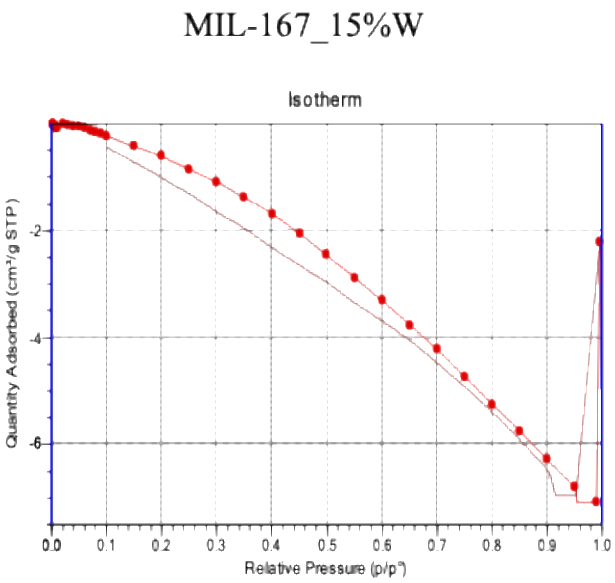

Figure 15. Nitrogen adsorption-desorption isotherms of MIL-167_15%W (sample mass: 50 mg)

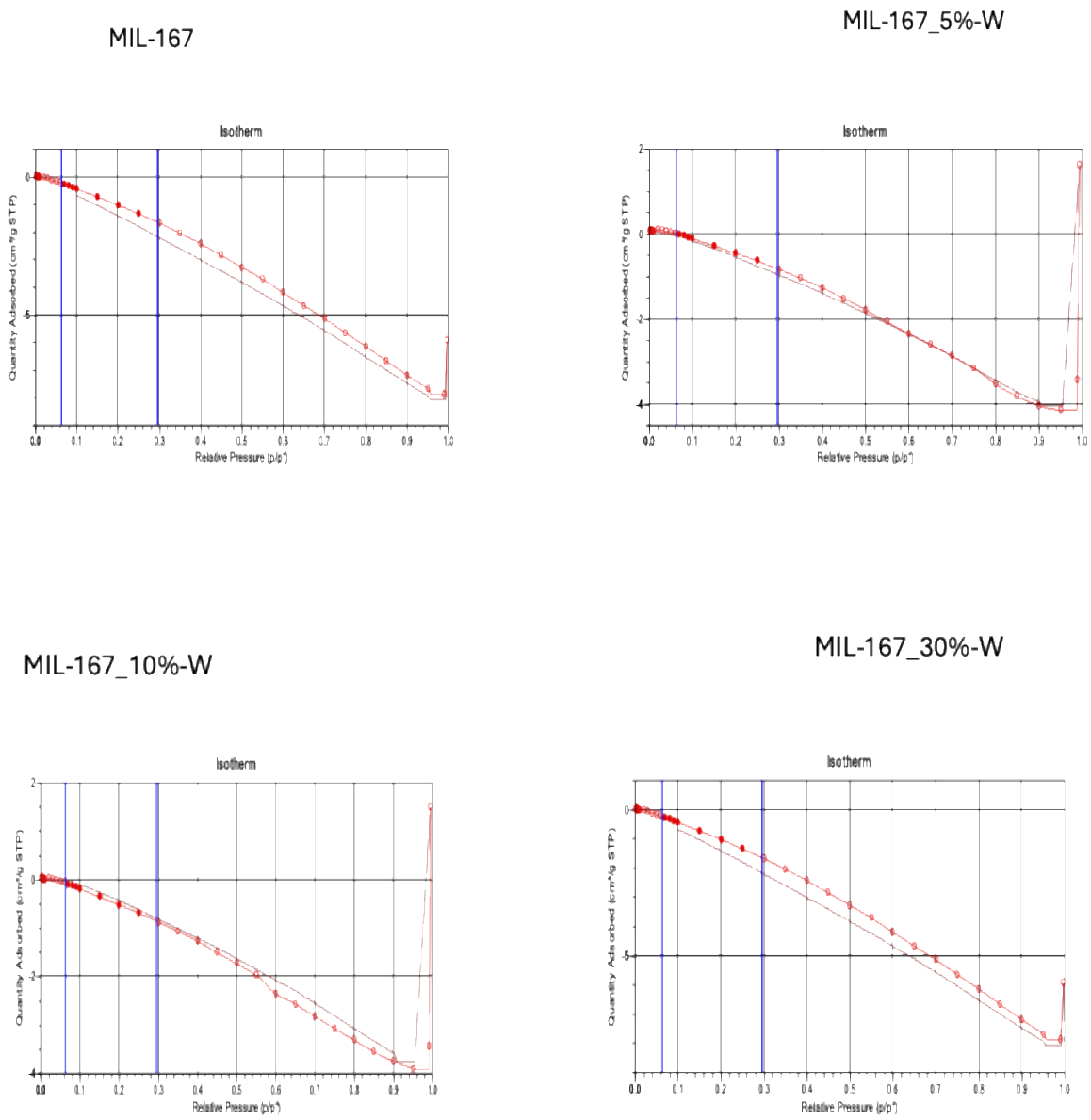

Figure 16. Nitrogen adsorption-desorption isotherms of MIL-167, MIL-167_5%_W, and MIL-167_10%_W, MIL-167_30%_W (sample mass: 100 mg).

As shown in Figure 15, the nitrogen isotherm of MIL-167-15%_W (50 mg sample mass) does not reach a plateau; instead, the uptake continues to increase gradually at high relative pressure, and the curve appears to decline or show instability. Similarly, Figure 16 shows the nitrogen isotherms for MIL-167, MIL-167-5%_W, MIL-167-10%_W, and MIL-167-30%_W, each measured with a sample mass of 100 mg. All four samples deviate from the expected Type I shape. Instead of reaching a flat plateau, the isotherms exhibit a downward trend or irregular

shape at higher relative pressures. This behavior is not consistent with a well-defined microporous material when using N_2 at 77 K.

Several hypotheses may explain the observed behavior for the W-doped MIL-167 samples. First, the pores of MIL-167 and its W-doped derivatives may be too narrow (ultramicroporous) to allow significant N_2 uptake at 77 K. Second, the pores may be partially or fully blocked by residual solvent molecules that were not completely removed during the degassing procedure, despite the activation conditions employed. Third, the introduction of tungsten during synthesis may lead to pore blockage.

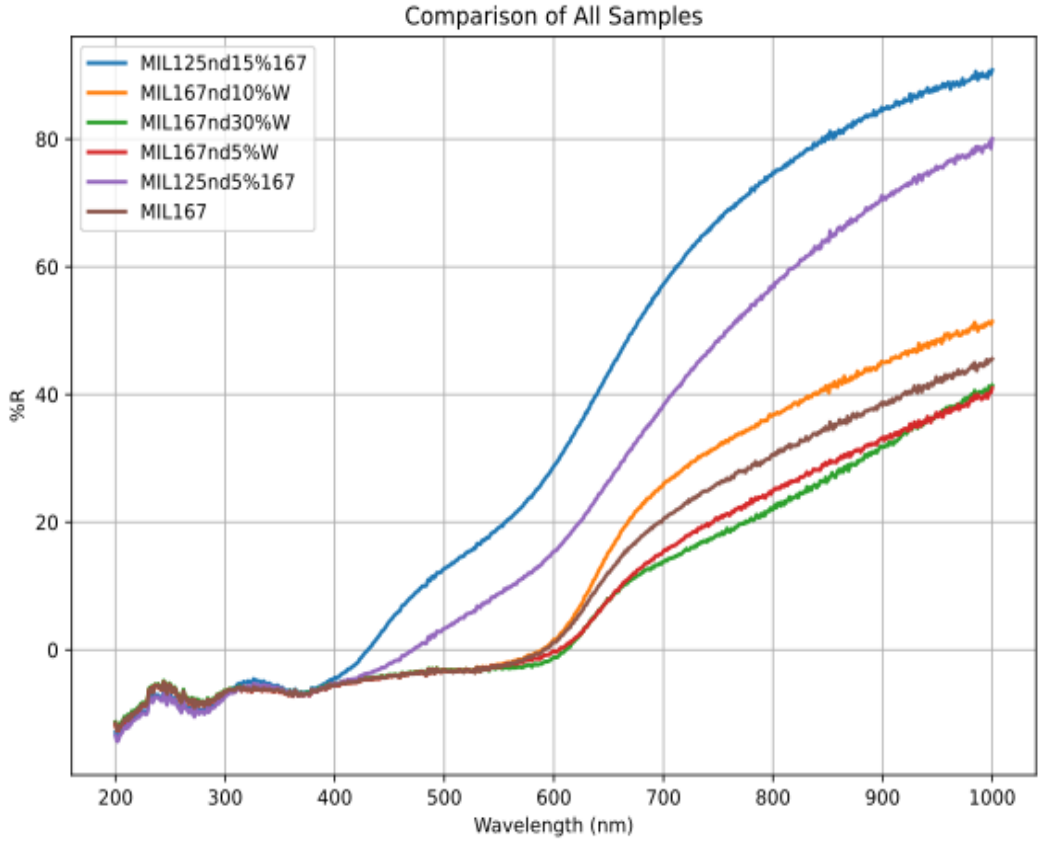

Figure 17. Reflectance spectra of MIL-167 and MIL-125/W-doped-MIL-167 heterojunctions.

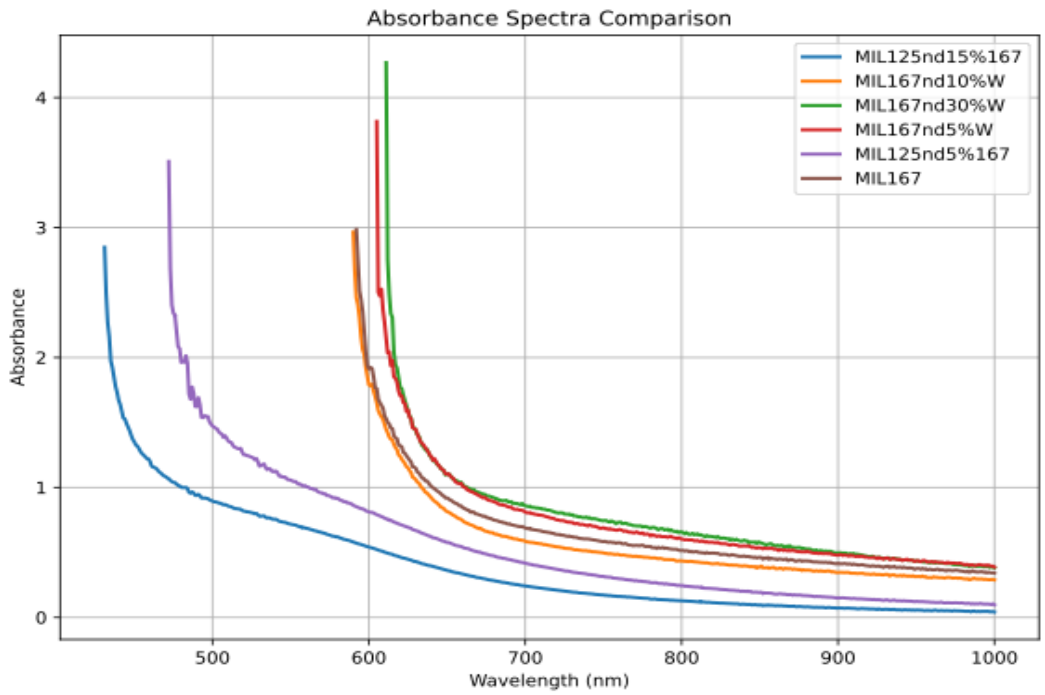

Figure 18. Absorbance spectra of MIL-167 and MIL-125/W-doped-MIL-167 heterojunctions.

To examine the impact of metal node substitution on the electronic structure of the synthesized frameworks, ultraviolet-visible (UV-Vis) diffuse reflectance spectroscopy (DRS) was conducted using a Cary 60 spectrophotometer equipped with a diffuse reflectance accessory. The measured wavelength range (200–1000 nm) covers both the ultraviolet (UV, 200–400 nm) and visible (Vis, 400–800 nm) regions, extending into the near-infrared (NIR, 800–1000 nm). Within this range, electronic transitions occur as electrons from the framework are promoted across energy states by absorbing photons [34].

The primary goal of partially substituting titanium with tungsten in the MIL-167 framework is band gap engineering, aimed at enhancing photocatalytic or photovoltaic performance. Tungsten possesses different d-electron configurations compared to titanium. Substituting Ti with W may introduce new electronic states into the MOF's band structure, potentially lowering the band gap energy and enabling absorption of lower-energy visible light. Additionally, mixed-metal MOFs can form local heterojunctions [30] or alter electron mobility within the framework, thereby reducing electron-hole recombination rates and increasing photochemical activity.

To enable direct comparison of absorption behavior from diffuse reflectance data, the reflectance spectra were converted to pseudo-absorbance using the Kubelka–Munk function (Eq. 3). This transformation is essential for scattering-dominated powder samples, as it linearizes the relationship between reflectance and absorption coefficient.

In the UV region, all samples exhibit very low reflectance as shown in Figure 17, which corresponds to high absorbance after Kubelka–Munk conversion revealed in Figure 18. This indicates that all frameworks strongly absorb UV light, consistent with intrinsic electronic transitions of the organic linkers and metal-oxo clusters.

The absorption onset is identified where the reflectance curve begins to rise sharply (or where $F(R_\infty)$ begins to drop). Samples indicated by blue and purple lines start rising much earlier (around 400 nm), meaning they cease absorbing visible light and begin reflecting it at shorter wavelengths, implying a wider band gap.

In contrast, samples indicated by orange, green, red, and brown lines exhibit absorption edges shifted significantly toward higher wavelengths (lower energies). Their reflectance remains flat and low—indicating sustained absorption—until approximately 550–600 nm before rising. This redshift in the absorption edge confirms a narrower band gap, favorable for visible-light harvesting.

Pristine MIL-167 (brown line) serves as the baseline. The 5% W (red line) and 30% W (green line) samples consistently lie below the pristine curve in the visible/NIR region (600–1000 nm). Lower reflectance (and correspondingly higher $F(R_\infty)$) indicates enhanced absorption across the visible spectrum. This confirms that incorporating 5% and 30% W successfully extends the light absorption range, improving the material's ability to harvest visible and near-infrared photons.

However, the 10% W sample (orange line) shows higher reflectance than pristine MIL-167 across most of the visible range. This unexpected behavior may point to experimental variance during synthesis (e.g., incomplete substitution, phase segregation, or differences in particle size/morphology) rather than a monotonic trend.

Samples formed by combining MIL-167 with MIL-125-NH_2 (heterojunction) exhibit distinctly different UV-Vis reflectance behavior compared to both pristine and W-modified MIL-167. These differences suggest that heterojunction formation alters charge transfer pathways and optical absorption profiles, meriting further investigation into their potential for photocatalytic applications.

3.1. Functional Application

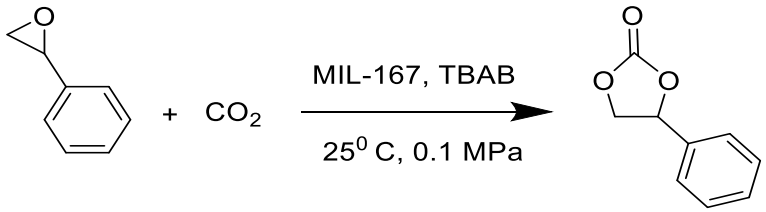

Scheme 2. Catalytic conversion of CO_2 to cyclic carbonate

The cycloaddition of CO_2 to epoxides using a Lewis acidic MOF and TBAB as a co-catalyst follows the established pathway outlined below [33, and references therein]:

Epoxide Coordination (Activation)

The oxygen atom of the highly strained oxirane ring (styrene oxide) coordinates to a vacant Lewis acidic metal center within the MIL-167 framework. This coordination polarizes the C–O bonds of the epoxide, increasing the electrophilicity of the ring carbon atoms.

Nucleophilic Ring Opening

The bromide ion from the TBAB co-catalyst acts as a nucleophile and attacks the less sterically hindered carbon atom of the activated epoxide ring. This nucleophilic attack opens the strained three-membered ring, generating a stable, metal-coordinated halo-alkoxide intermediate.

Carbon Dioxide Insertion

The nucleophilic oxygen atom of the newly formed halo-alkoxide intermediate attacks the electrophilic carbon atom of a nearby CO_2 molecule. This reversible insertion forms a linear metal-bound bromo-carbonate intermediate.

Intramolecular Cyclization and Catalyst Regeneration

The terminal carbonate oxygen atom undergoes rapid intramolecular nucleophilic displacement, attacking the same carbon atom that bears the bromide group. This expels the

bromide ion as a leaving group, forming the stable five-membered styrene carbonate ring. The product dissociates from the metal center, simultaneously regenerating both the MIL-167 active site and the TBAB co-catalyst for the next catalytic cycle.

The catalytic efficiency of the MIL-167/TBAB system for the cycloaddition of CO_2 to styrene oxide was evaluated via ^1H NMR spectroscopy after reaction periods of 24 and 48 hours, with the spectra collected in Figures S1 and S2, respectively, in the supporting Information.

As shown in Figures S1 and S2, the formation of styrene carbonate was confirmed by the appearance of a triplet at δ 5.55 ppm (1H, CH) and a pair of doublets of doublets at δ 4.65 ppm and δ 4.20 ppm (2H, CH_2). These signals are characteristic of the methine and methylene protons, respectively, of the cyclic carbonate ring.

The oxirane ring protons of the unreacted styrene oxide starting material appear as three non-equivalent protons. The methine proton attached to the phenyl ring is observed as a doublet of doublets at δ 3.70 ppm (dd, 1H). The two diastereotopic methylene protons appear as complex multiplets between δ 2.75–3.15 ppm (2H, m).

The peak at δ 7.26 ppm is the residual $CHCl_3$ from deuterated chloroform solvent. The aromatic protons overlap heavily in this region.

The conversion of styrene oxide to styrene carbonate was determined by comparing the integrated areas of two single-proton resonances: the methine proton of the cyclic carbonate product (δ 5.55 ppm, 1H) and the methine proton of the unreacted epoxide starting material (δ 3.70 ppm, 1H). Because both signals correspond to exactly one proton each, their integration ratio directly gives the molar ratio of product to remaining starting material.

The yield of styrene carbonate was calculated using the mole fraction method:

$$\text{Yield (\%)} = \frac{I_{\text{product}}}{I_{\text{product}} + I_{\text{starting}}} \times 100 \qquad (4)$$

After 48 hours of reaction (Figure S2), the integration ratio of product to starting material (δ 5.55 ppm: δ 3.70 ppm) was determined to be 1:1 from the measured peak areas. Substituting $I_{\text{product}} = 1$ and $I_{\text{starting}} = 1$ into Eq. (4) gives a yield of 50%.

In conclusion, the formation of styrene carbonate was confirmed by the appearance of a triplet at δ 5.55 ppm, corresponding to the strongly deshielded methine (CH) proton of the newly formed dioxolanone ring, together with a pair of doublets of doublets at δ 4.65 ppm and δ 4.20 ppm (2H, CH_2). Concurrently, unreacted styrene oxide was monitored via its oxirane ring methine proton at δ 3.70 ppm (doublet of doublets). Comparative integration of these two single-proton resonances revealed a product-to-starting-material ratio of 1:1 after 48 hours, corresponding to a yield of styrene carbonate of 50% under the employed reaction conditions.

4. Conclusion

In this study, MIL-167 was successfully synthesized, and its crystal structure was preserved under varying synthesis conditions, including changes in autoclave volume. Partial substitution of Ti with W at different molar ratios did not alter the crystal structure, as confirmed by X-ray diffraction, while X-ray fluorescence indicated the presence of tungsten in the samples. However, the exact location of W within the framework remains uncertain, and it is possible that tungsten species are partially located within the pores rather than being fully incorporated into the framework nodes. Spectroscopic and thermal analyses revealed no major structural differences between pristine and W-modified MIL-167, suggesting that the framework remains largely unchanged upon modification.

The absence of crystalline product in the synthesis without methanol highlights the critical role of methanol in the formation of MIL-167, likely through its involvement in hydrolysis, coordination, and nucleation processes during solvothermal synthesis. Functional studies revealed that W doping did not enhance the expected properties: nitrogen physisorption results suggested inaccessible porosity, potentially due to pore blockage or reduced pore size. However, some catalytic activity was observed in the cycloaddition of CO_2 to epoxides. Additionally, UV–Vis studies indicated altered optical behavior in heterojunction systems, though further investigation is required to establish their photocatalytic relevance.

Overall, while tungsten incorporation was achieved to some extent, it did not lead to significant improvements in structural or functional properties. Future work should focus on improving metal incorporation into the framework nodes, optimizing synthesis conditions—particularly solvent composition—and exploring alternative strategies to enhance porosity and catalytic performance.

References

[1] Zhang, X.; Chen, Z.; Liu, X.; Hanna, S. L.; Wang, X.; Taheri-Ledari, R.; Maleki, A.; Li, P.; Farha, O. K. *Chem. Soc. Rev.* **2020**, *49*, 7406–7427.

[2] Davis, M. E. *Nature* **2002**, *417*, 813–821.

[3] Davis, M. E.; Saldarriaga, C.; Montes, C.; Garces, J.; Crowdert, C. *Nature* **1988**, *331*, 698–699.

[4] Kresge, C. T.; Leonowicz, M. E.; Roth, W. J.; Vartuli, J. C.; Beck, J. S. *Nature* **1992**, *359*, 710–712.

[5] Yaghi, O. M.; Li, H. *J. Am. Chem. Soc.* **1995**, *117*, 10401–10402.

[6] Yaghi, O. M.; Li, G.; Li, H. *Nature* **1995**, *378*, 703–706.

[7] Li, H.; Eddaoudi, M.; Groy, T. L.; Yaghi, O. M. *J. Am. Chem. Soc.* **1998**, *120*, 8571–8572.

[8] Eddaoudi, M.; Kim, J.; Rosi, N.; Vodak, D.; Wachter, J.; O'Keeffe, M.; Yaghi, O. M. *Science* **2002**, *295*, 469–472.

[9] Gropp, C.; Canossa, S.; Wuttke, S.; Gándara, F.; Li, Q.; Gagliardi, L.; Yaghi, O. M. *ACS Cent. Sci.* **2020**, *6*, 1255–1273.

[10] Li, A.; Bueno-Perez, R.; Wiggin, S.; Fairen-Jimenez, D. *CrystEngComm* **2020**, *22*, 4512–4521.

[11] Moghadam, P. Z.; Li, A.; Wiggin, S. B.; Tao, A.; Maloney, A. G. P.; Wood, P. A.; Ward, S. C.; Fairen-Jimenez, D. *Chem. Mater.* **2017**, *29*, 2618–2625.

[12] IUPAC. *Pure Appl. Chem.* **2013**, *85*, 1715.

[13] Kondo, M.; Yoshitomi, T.; Matsuzaka, H.; Kitagawa, S.; Seki, K. *Angew. Chem., Int. Ed. Engl.* **1997**, *36*, 1725–1727.

[14] Farha, O. K.; Hupp, J. T. *Acc. Chem. Res.* **2010**, *43*, 1166–1175.

[15] Howarth, A. J.; Peters, A. W.; Vermeulen, N. A.; Wang, T. C.; Hupp, J. T.; Farha, O. K. *Chem. Mater.* **2017**, *29*, 26–39.

[16] Kaye, S. S.; Dailly, A.; Yaghi, O. M.; Long, J. R. *J. Am. Chem. Soc.* **2007**, *129*, 14176–14177.

[17] Llewellyn, P. L.; Bourrelly, S.; Serre, C.; Vimont, A.; Daturi, M.; Hamon, L.; De Weireld, G.; Chang, J.-S.; Hong, D.-Y.; Hwang, Y. K.; Hwa Jhung, S.; Férey, G. *Langmuir* **2008**, *24*, 7245–7250.

[18] Nelson, A. P.; Farha, O. K.; Mulfort, K. L.; Hupp, J. T. *J. Am. Chem. Soc.* **2009**, *131*, 458–460.

[19] Kumari, S.; Gusain, M.; Lamba, B. Y.; Kumar, S. *J. Mater. Chem. A* **2025**, *13*, 21352–21368.

[20] Safaei, M.; Foroughi, M. M.; Ebrahimpoor, N.; Jahani, S.; Omidi, A.; Khatami, M. *TrAC, Trends Anal. Chem.* **2019**, *118*, 401–425.

[21] Tranchemontagne, D. J.; Tranchemontagne, J. L.; O'Keeffe, M.; Yaghi, O. M. *Chem. Soc. Rev.* **2009**, *38*, 1257–1283.

[22] Raptopoulou, C. P. *Materials* **2021**, *14*, 310.

[23] Assi, H.; Pardo Pérez, L. C.; Mouchaham, G.; Ragon, F.; Nasalevich, M.; Guillou, N.; Martineau, C.; Chevreau, H.; Kapteijn, F.; Gascon, J.; Fertey, P.; Elkaim, E.; Serre, C.; Devic, T. *Inorg. Chem.* **2016**, *55*, 7192–7199.

[24] Li, D.; Yadav, A.; Zhou, H.; Roy, K.; Thanasekaran, P.; Lee, C. *Global Challenges* **2024**, *8*, 2300244.

[25] Encyclopedia Britannica. Titanium (Ti) – Chemical Properties. 2024. Available at: https://www.britannica.com/science/titanium (Accessed: May 28, 2026).

[26] Wikipedia contributors. Tungsten. *Wikipedia, The Free Encyclopedia*. Available at: https://en.wikipedia.org/wiki/Tungsten (Accessed: May 28, 2026).

[27] Chemistry LibreTexts. Group 6: Transition Metals. Available at: https://chem.libretexts.org (Accessed: May 28, 2026).

[28] Shannon, R. D. *Acta Crystallogr., Sect. A* **1976**, *32*, 751–767.

[29] Thommes, M.; Kaneko, K.; Neimark, A. V.; Olivier, J. P.; Rodriguez-Reinoso, F.; Rouquerol, J.; Sing, K. S. W. *Pure Appl. Chem.* **2015**, *87*, 1051–1069.

[30] Kampouri, S.; Ebrahim, F. M.; Fumanal, M.; Nord, M.; Schouwink, P. A.; Elzein, R.; Addou, R.; Herman, G. S.; Smit, B.; Ireland, C. P.; Stylianou, K. C. *ACS Appl. Mater. Interfaces* **2021**, *13*, 14239–14247.

[31] IUPAC. Kubelka–Munk function. In *IUPAC Compendium of Chemical Terminology (The Gold Book)*, Version 5.0.0, 2025. Available at: https://goldbook.iupac.org/terms/view/08631 (Accessed: May 28, 2026).

[32] Wang, H. H.; Hou, L.; Li, Y. Z.; Jiang, C. Y.; Wang, Y. Y.; Zhu, Z. *ACS Appl. Mater. Interfaces* **2017**, *9*, 17969–17976.

[33] Lehtonen, A.; Sillanpää, R. *Polyhedron* **1994**, *13*, 2519–2524.

[34] Minchiotti, M. C. In *Infrared Spectroscopy - Biotechnological Applications*; IntechOpen, 2024.

Supporting information

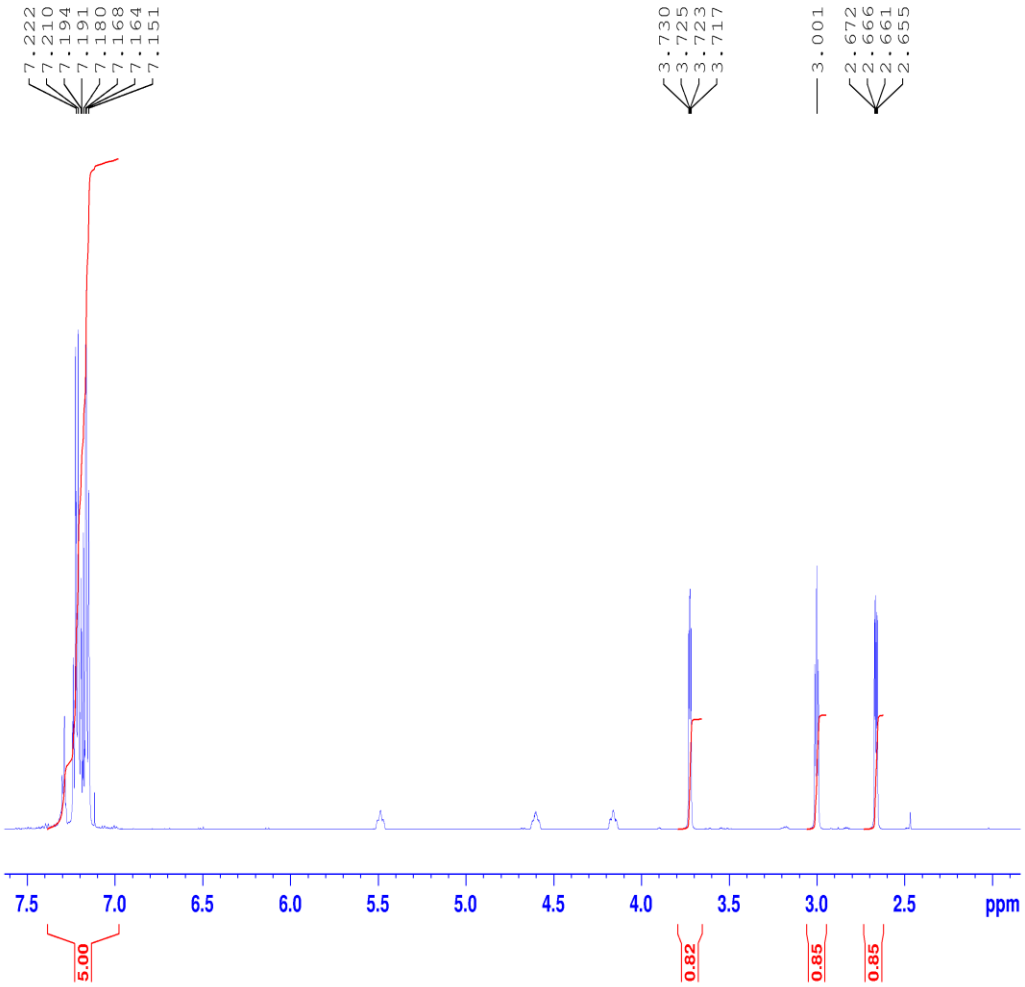

Figure S1. ^{1}H NMR spectrum of reaction for the conversion of styrene oxide to styrene carbonate after 24 h

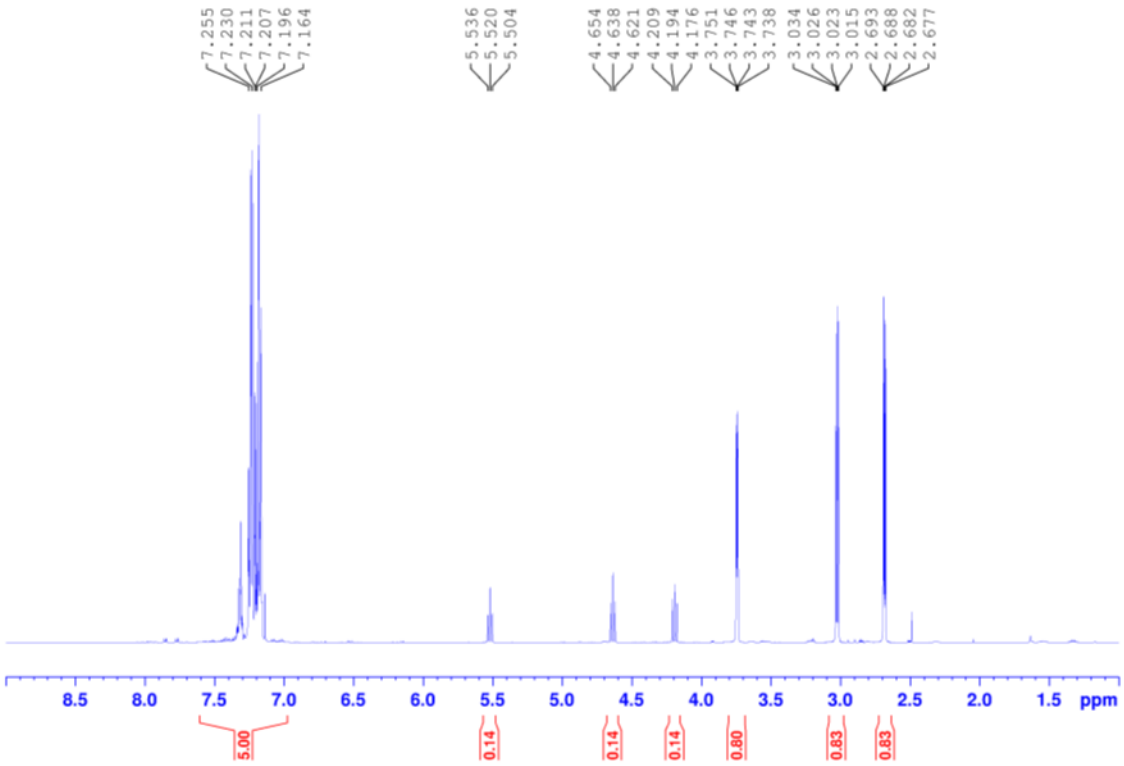

Figure S2. ^{1}H NMR spectrum of reaction for the conversion of styrene oxide to styrene carbonate after 48 h